

Optical properties of Fermi polarons in a $\text{GaInP}/\text{MoSe}_2$ monolayer heterostructure

Hangyong Shan¹, Max Waldherr², Diksha Diksha¹, Ghada Missaoui¹, Seyma Esra Atalay¹, Martin Zinner², Ana Maria Valencia¹, Kenji Watanabe⁴, Takashi Taniguchi⁵, Seth Ariel Tongay³, Caterina Cocchi^{1,9}, Brendan C. Mulkerin⁶, Jesper Levinsen⁶, Francesca Maria Marchetti^{7,8}, Meera M. Parish⁶, Niklas Nilius¹, Christian Schneider^{1,†}, Sven Höfling²

¹*Institute of Physics, Faculty V, and Center for Nanoscale Dynamics (CeNaD), Carl von Ossietzky University Oldenburg, 26129 Oldenburg, Germany*

²*Technische Physik and Wilhelm-Conrad-Röntgen-Research Center for Complex Material Systems, Universität Würzburg, D-97074 Würzburg, Am Hubland, Germany*

³*Materials Science and Engineering, School for Engineering of Matter, Transport, and Energy, Arizona State University, Tempe, Arizona 85287, USA*

⁴*Research Center for Electronic and Optical Materials, National Institute for Materials Science, 1-1 Namiki, Tsukuba 305-0044, Japan*

⁵*Research Center for Materials Nanoarchitectonics, National Institute for Materials Science, 1-1 Namiki, Tsukuba 305-0044, Japan*

⁶*School of Physics and Astronomy, Monash University, Victoria 3800, Australia*

⁷*Departamento de Física Teórica de la Materia Condensada, Universidad Autónoma de Madrid, Madrid 28049, Spain*

⁸*Condensed Matter Physics Center (IFIMAC), Universidad Autónoma de Madrid, 28049 Madrid, Spain*

⁹*Friedrich-Schiller University Jena, Institute for Condensed Matter Theory and Optics, 07743 Jena, Germany*

[†]*Corresponding author. Email: christian.schneider@uol.de*

Abstract:

Engineering optical properties, such as luminescence purity and charge transfer, is crucial for harnessing the application potential of atomically thin transition metal dichalcogenides (TMDCs). While electrostatic gating is widely applied to gain charge control in TMDC monolayers, charge transfer can also be engineered via coupling of TMDC monolayers at semiconductor III/V, organic, or van der Waals interfaces. This confers great advantages, such as ease in implementation and compatibility in device integration. Here, we shed light on the optical properties of many-particle complexes emerging at the $\text{GaInP}/\text{MoSe}_2$ interface as a highly relevant material combination to manipulate the optical properties of TMDCs in integrated photonic devices. Our study verifies its nature as a type II hetero-interface, which bears the feasibility to display disorder-free photoluminescence. Through optical absorption measurements, we verify that the charged complexes acquire substantial oscillator strength. Furthermore, temperature-dependent photoluminescence, supported by a microscopic theory framework, evidences the suppression of the characteristic carrier recoil effect that was previously observed in the photoluminescence of trions in TMDCs. These phenomena allow us to identify the optical signatures at the TMDC-GaInP interface as Fermi polaron quasiparticle resonances, which are of high importance in researching Bose-Fermi mixtures in condensed matter systems.

Introduction

Atomically thin transition metal dichalcogenides (TMDCs) have emerged as an excellent platform to study fundamental effects of light-matter coupling and exciton physics in low dimensions¹, and to explore correlated quantum states of matter^{2, 3}. Being van der Waals materials, TMDC monolayers and heterostructures are extremely versatile regarding their integration with electronic⁴ and photonic⁵ device structures, which explains their tremendous application potential. However, due to their ultimate thinness, the structural surrounding of a TMDC monolayer, such as the choice of the substrate material, widely influences its optoelectronic properties via several effects, including photonic coupling, dielectric screening, disorder, and charge transfer⁶⁻¹⁰. Consequently, it is of significant interest to shed light on the optical properties of device-relevant combinations of TMDCs with commonly used materials in optoelectronic research, such as III/V semiconductors.

A variety of hybrid III/V-TMDC structures has already been employed in photonic applications, including hybrid polariton lasers¹¹ and other nanophotonic devices¹², where excitonic effects in TMDCs dominate the optical response. Further studies have characterized excitons at the TMDCs-semiconductor interface from a fundamental perspective⁹. Besides excitons, charged complexes such as trions are observed in TMDCs due to strong Coulomb interactions^{13, 14}. Trion resonances can become very prominent when TMDC monolayers are integrated with carrier-donating substrates^{15, 16}, which also attract particular interest due to their fermionic nature¹⁷. When the free carrier density becomes greater than the exciton density, excitons can be regarded as quantum impurities immersed in a Fermi sea. Within this picture, excitons and trions evolve into repulsive (RP) and attractive Fermi polarons (AP) respectively, where excitons either repel or attract the surrounding Fermi particles¹⁸⁻²². The optical properties of Fermi polarons in atomically thin semiconductors – such as their emission frequency, dephasing properties, and oscillator strength – strongly depend on the doping density^{19, 21, 22}, which can be modified either by electric gates or various substrates.

The Fermi polaron represents a ubiquitous scenario in physics, with realizations spanning a wide range of platforms, from ultracold atomic gases²³, to high-energy and condensed-matter systems²⁴. Major advances in the context of atomically thin semiconductors include the observation of a strongly enhanced nonlinear optical response²⁵, as well as the controlled manipulation of exciton–polaron states using external electric^{26, 27} and magnetic fields²⁷. Recently, polaron states have also attracted significant interest as sensitive probes of strongly correlated electronic phases, such as Wigner crystals²⁸⁻³⁰, quantum Hall states²⁰, correlated Mott insulating states emerging in moiré superlattices³¹, as well as spin sensors of correlated topological phases³².

In this work, we scrutinize the optical properties of many-body complexes at the interface between monolayer MoSe₂ and epitaxially grown GaInP crystals, both among the most technologically relevant representatives of TMDCs and III/V semiconductors, respectively^{4, 33}. The optical bandgap of GaInP (lattice-matched to GaAs with the chemical composition Ga_{0.51}In_{0.49}P) is sufficiently large to make it compatible with the integration of various TMDC monolayers and bilayers, in stark contrast to, e.g., GaAs or Si. Earlier reports have furthermore hinted that the dielectric properties of GaInP yield high-brightness emission of charged carrier complexes from TMDCs in their proximity^{7, 15, 34, 35}. Here, we combine scanning tunneling spectroscopy, photoluminescence (PL), and optical absorption measurements to detail the energy landscape at the GaInP/MoSe₂ hybrid interface. We observe unambiguous spectral fingerprints of coherent

Fermi polaron quasiparticles, including significant optical absorption of the charged carrier complex, and the absence of the carrier recoil effect at elevated temperatures.

Results and Discussion

The sample structure is shown in Fig. 1a. The GaInP layer is grown on a distributed Bragg reflector (DBR). The MoSe₂ monolayers and hexagonal boron nitride (hBN) layers are exfoliated from crystals, and deposited via a standard dry viscoelastic transfer method. See more details of sample preparations in Methods. First, we analyze the band-configuration of the hybrid GaInP/MoSe₂ interface that is essential to understand the optical signatures and fingerprints. We therefore conduct low-temperature (100 K) scanning tunneling microscope (STM) experiments under ultra-high vacuum conditions, utilizing an exfoliated MoSe₂ monolayer on a GaInP surface. The top inset of Fig. 1a displays a topographic image of the MoSe₂ monolayer on GaInP with atomic resolution. The MoSe₂ monolayer clearly reveals the hexagonal pattern of the topmost Se plane with 3.2 Å periodicity³⁶.

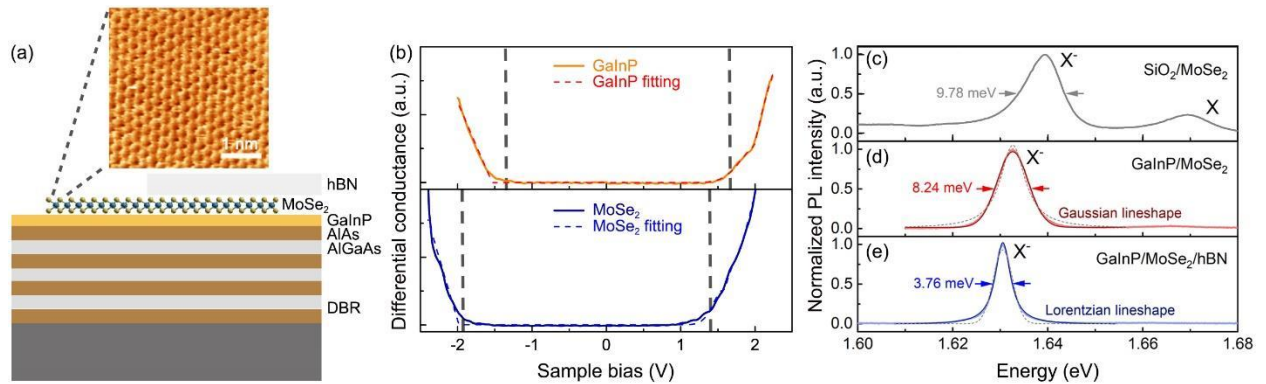


Figure 1 (a) Schematic drawing of the investigated GaInP/MoSe₂ sample, with an STM tomographic image of MoSe₂ monolayer on GaInP surface. (b) Differential conductance spectra taken at MoSe₂ monolayer and GaInP (Setpoint 2.0 V, 0.1 nA). Normalized photoluminescence spectra recorded at T = 4 K of (c) uncovered MoSe₂ on a SiO₂ substrate, (d) uncovered and (e) hBN-covered MoSe₂ on a GaInP substrate, respectively. (c) On SiO₂, we observe a pronounced trion peak in photoluminescence (X') and a weaker exciton peak (X). (d) On GaInP, we observe almost no emission from the exciton, while the remaining luminescence peak (X') has a Gaussian line shape (dark red line). The dashed line represents a Lorentzian fit, underlining the deviation of the measured signal from this lineshape. (e) Upon covering the flake with a thin layer of hBN, the emission shifts to slightly lower energies, and the linewidth drops considerably. The spectrum is in almost perfect agreement with a Lorentzian fit (dark blue line). In contrast to (d), the Gaussian fit (dashed line) does not reproduce the spectrum.

Differential conductance (dI/dV) spectra are acquired to probe the band positions of the GaInP substrate and the MoSe₂ monolayer with respect to the Fermi level. Example spectra for each surface are depicted in Fig. 1b; they are fitted with linear slopes to determine the band edges and a Gaussian function to account for possible gap states. A statistical average for the band onsets has been derived from several dozens of spectra, and the respective mean values of the valence band (VB) and conduction band (CB) onset are indicated as dashed lines in Fig. 1b. The GaInP shows a nearly symmetric bandgap with VB and CB onsets at -1.3 ± 0.3 V and $+1.7 \pm 0.3$ V, respectively, as well as a surface state at ~ 1.3 V³⁷. We note that the measured band gap is larger

than literature values for the $\text{Ga}_{0.5}\text{In}_{0.5}\text{P}$ composition³⁸, most likely due to band bending effects in the tip electric field. Also, the intrinsic n-type conductance behavior seems to be washed out, probably due to a naturally evolving surface passivation layer. As a comparison, the MoSe_2 monolayer has a clearly downshifted bandgap with VB and CB onsets at -1.9 ± 0.2 V and $+1.4 \pm 0.3$ V, respectively. Thus, the detected band alignment corresponds to a type II hetero-interface between GaInP and the MoSe_2 monolayer, where the CB confines electrons in MoSe_2 , leaving holes effectively unconfined. Additionally, we make use of density functional theory (DFT) – a powerful tool to study electronic and optical properties of TMDC monolayers^{39, 40} – to confirm a type II band alignment of the $\text{GaInP}/\text{MoSe}_2$ heterostructure (Fig. S1), in agreement with the result of differential conductance spectra. Particularly, the lowest unoccupied level being localized in the MoSe_2 promotes efficient electron transfer across the interface into the TMDC monolayer.

To probe the optical properties, we record low-temperature (4K) PL spectra at different positions on three samples: (i) uncovered MoSe_2 monolayer on a SiO_2 substrate, (ii) uncovered and (iii) hBN-covered MoSe_2 monolayer on a GaInP substrate. Representative spectra for each group are shown in Fig. 1c-e and display significant variations in their response due to the different dielectric environments of the TMDC monolayer. As shown in Fig. 1c, the PL spectrum of MoSe_2 on a SiO_2 substrate features two prominent broad peaks that can be readily attributed to resonances connected to the exciton and trion of MoSe_2 monolayer in the presence of modest charging. The trion peak takes up around 85% of the total emission, suggesting an accumulation of carriers in the TMDC layer. In addition, the lineshape of the trion luminescence fits neither a Gaussian nor Lorentzian profile. This phenomenon can be understood as a result of the electron recoil effect⁴¹⁻⁴³, as we discuss further below.

In stark contrast, the exciton resonance vanishes almost completely in PL spectra recorded from the MoSe_2 monolayer on a GaInP substrate (Fig. 1d). This behaviour, which has been previously reported in Ref.¹⁵, suggests an efficient charge transfer at the $\text{GaInP}/\text{MoSe}_2$ interface resulting in heavy doping of the TMDC monolayer. The PL signal clearly exhibits a Gaussian lineshape with a full width at half maximum (FWHM) of 8.3 meV, evidencing a reduction of large-scale inhomogeneities compared to the $\text{SiO}_2/\text{MoSe}_2$ interface. The dashed grey line in Fig. 1d shows an alternative Lorentzian fit for comparison, and its poor match to the spectrum underlines the Gaussian distribution of the measured data. Moreover, in comparison to the $\text{SiO}_2/\text{MoSe}_2$ sample, the $\text{GaInP}/\text{MoSe}_2$ emission signal undergoes a redshift of ~ 7.6 meV, being explained by the modified dielectric environment and an energy renormalization arising from increased correlations at heavy doping conditions.

Upon placing a thin layer of hBN on top of the MoSe_2 flake and annealing it at 400 °C in an Ar:H_2 atmosphere (95:5 ratio), we observe further modifications in the optical properties of our samples. Apart from a modest red shift by 0.5 meV, most importantly, we notice a transition to a Lorentzian lineshape, indicating a reduction of inhomogeneities. In Fig. 1e, we include an alternative Gaussian fit (dashed line) to show an inferior match to the measured data and illustrate the almost perfect Lorentzian lineshape of the spectrum. Intriguingly, the recorded optical linewidth narrows down to a value as low as 3.8 meV, corroborating the strongly suppressed inhomogeneous broadening effects. We note that, although narrow-band photoluminescence upon full hBN encapsulation of TMDC monolayers has been observed in many labs^{35, 44, 45}, such high-quality emission features with exceptionally small FWHM are only sparsely documented in hybrid heterostructures⁹.

To back up our findings statistically, we plot the extracted linewidths of the photoluminescence peak from the tentatively assigned charged complex with 0.5 meV binning in a histogram (Fig. 2a). The progressive reduction of the average linewidth becomes immediately evident, when changing from SiO_2 to GaInP substrates and applying a hBN cover. For $\text{SiO}_2/\text{MoSe}_2$ and hBN-covered GaInP/ MoSe_2 , the linewidths spread over ~ 6 meV, while for uncovered GaInP/ MoSe_2 , they span a range of less than 2 meV, with an average value of 8.36 ± 0.44 meV. The enhanced linewidth fluctuation for the hBN-covered GaInP/ MoSe_2 sample can be explained by the improper contact between TMDCs and hBN cap in certain areas, due to the formation of bubbles during the transfer and annealing procedures. For these sample areas, the PL linewidth approaches the values of the uncapped sample.

The linewidth variance of GaInP/ MoSe_2 is smaller than that of $\text{SiO}_2/\text{MoSe}_2$ sample. This is in full agreement with a previous work¹⁵, where the linewidth of single photon emission in GaInP/WSe₂ has a smaller fluctuation than that of $\text{SiO}_2/\text{WSe}_2$. The reason behind them could be the same: the epitaxial grown substrate GaInP has better surface quality than SiO_2 substrate. Charge puddling is known to occur on SiO_2 surfaces, promoted by disorders such as dangling bonds and carrier traps, which causes stronger inhomogeneous broadening and linewidth fluctuation. Besides, the dielectric constant of SiO_2 is not as uniform as GaInP, contributing to a larger fluctuation of linewidth.

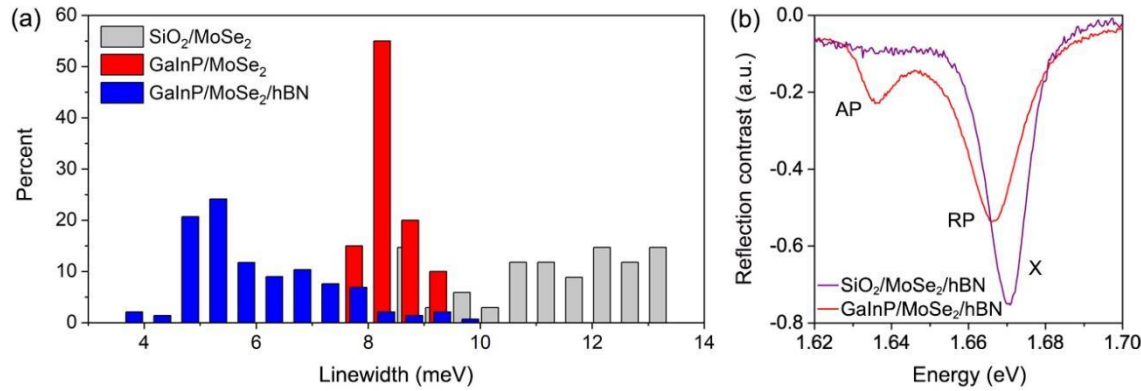


Figure 2 (a) Statistical analysis of the linewidth distribution of the MoSe_2 PL signal arising from the charged complex measured at different positions on the three samples. The measured linewidths are binned in 0.5 meV. On the SiO_2 substrate (gray bars), the linewidth is 11.31 meV in average and varies over a range of 5 meV. On the GaInP substrate (red bars), the linewidths lie within a range of 1.6 meV and the average linewidth is 8.36 meV. After covering the sample with a hBN thin layer (blue bars), the range of linewidths increases again to 5.76 meV, while the average linewidth narrows down to 5.95 meV and the linewidth can possibly reach a value as small as 3.76 meV. **(b)** White light reflection contrast spectra of a hBN-covered MoSe_2 flake on GaInP (red) and SiO_2 (purple). A strong absorption dip corresponds to the exciton resonance (X) for $\text{SiO}_2/\text{MoSe}_2/\text{hBN}$, whereas in GaInP/ MoSe_2/hBN spectra, a weaker absorption dip with lower energy indicates the emergence of attractive Fermi polaron (AP) complex, and the high energy absorption signal is assigned to the repulsive Fermi polaron (RP) counterpart.

In PL experiments on stochastically doped TMDC monolayers, the emergence of a lower energy peak is usually assigned to the formation of trions. However, the investigation of the oscillator strength via optical absorption allows us to draw more explicit conclusions. For this purpose, we carry out additional reflection measurements at 4 K, as depicted in Fig. 2b. The optical reflectivity of the $\text{SiO}_2/\text{MoSe}_2/\text{hBN}$ sample displays the standard behavior of ungated samples¹⁴: While the

assigned exciton peak features a very strong absorption signal, the absorption of the trion complex is strongly suppressed. This is in stark contrast to the observed behavior of our GaInP/MoSe₂/hBN samples: Here, we consistently observe two optical transitions with significant photo-absorption, whereby the low-energy absorption feature spectrally matches with the PL from the same sample as shown in Fig. 1e. The observation of strong oscillator strength of the charged carrier complex is especially striking, and allows us to assign the carrier complex to an emergent attractive Fermi polaron, with the higher energy absorption signal being its repulsive Fermi polaron counterpart^{20, 21}.

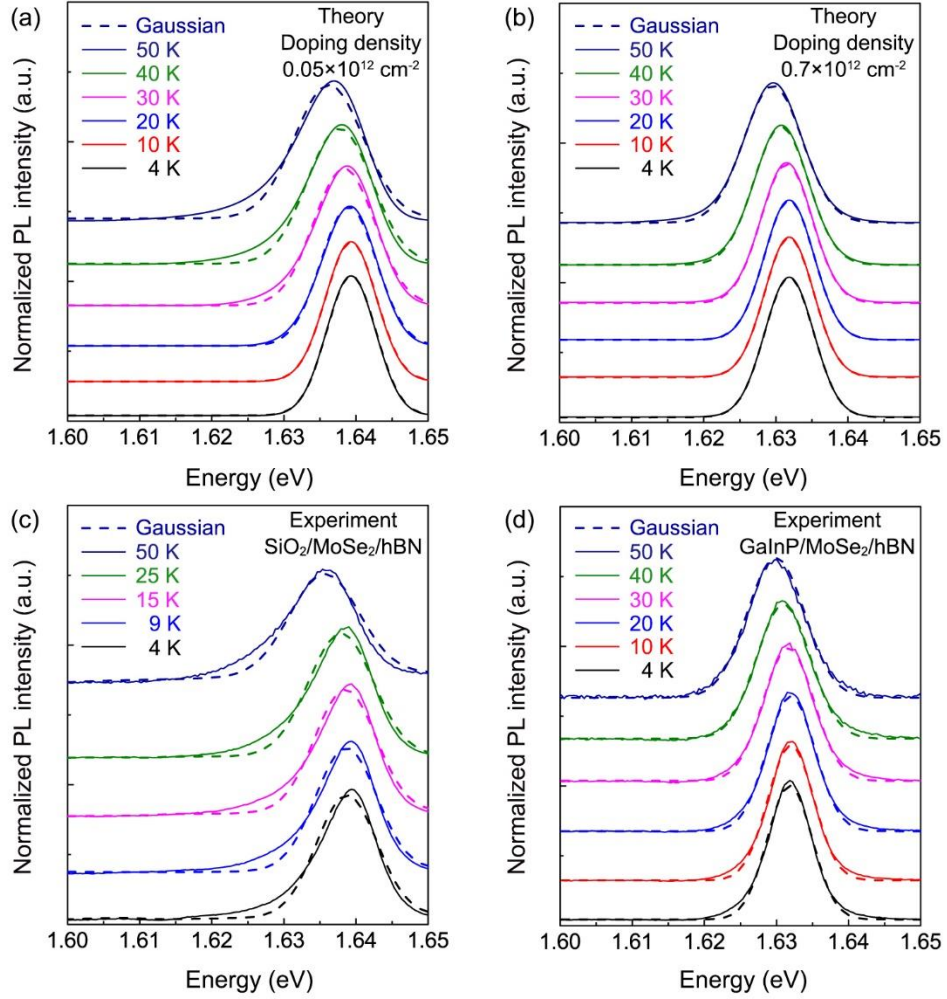


Figure 3 (a, b) Temperature evolution of the theoretical PL emission spectra of the charged complex in MoSe₂ monolayer evaluated at two different densities: **(a)** $0.05 \times 10^{12} \text{ cm}^{-2}$ and **(b)** $0.7 \times 10^{12} \text{ cm}^{-2}$. The doping density in **(b)** has been estimated by comparing the experimental and theoretical temperature dependence of the repulsive and attractive polaron energy splitting for the GaInP/MoSe₂/hBN sample (see Fig. S2). The dashed lines are Gaussian fittings to the theoretical profiles. **(c)** Experimental temperature dependent PL of the assigned trion signal in the SiO₂/MoSe₂/hBN stack, displaying a pronounced asymmetry at finite temperature due to the carrier recoil effect. **(d)** Experimental temperature dependent PL of the assigned attractive polaron signal in the GaInP/MoSe₂/hBN stack, retaining its symmetry over the entire temperature range from 4 - 50 K. All dashed curves are Gaussian fittings.

Besides a substantially different absorption behavior, AP complex and bound trion also differ in their temperature-dependent photoluminescence. To elucidate the distinction between attractive Fermi polaron and trion from the PL lineshapes, we calculate the PL within a finite-temperature non-perturbative Green's function approach^{46, 47}. Crucially, our theoretical framework captures the crossover⁴⁷ between an incoherent trion continuum at low charge densities $E_F \ll k_B T$ and a coherent Fermi-polaron quasiparticle at high densities $E_F \gg k_B T$, where T is the temperature and E_F is the Fermi energy associated with the doping of charges. Here, the attractive Fermi polaron in the quantum-degenerate regime leads to a symmetric emission profile, while at high temperature or low doping the attractive polaron quasiparticle is destroyed, merging with the broad trion-hole continuum. It leads to an asymmetric profile with an exponential tail, involving recoil charge carriers such as electrons at finite momentum. This phenomenon is known as the carrier recoil effect, which has been observed in charge tunable MoSe₂ monolayer under modest doping conditions⁴¹.

This is clearly observed in Fig. 3a, b, where we present the lineshape evolution of the charged complex (trion or AP) in the MoSe₂ monolayer as a function of temperature at two fixed densities. In Fig. 3a, we fix the density to a small value $0.05 \times 10^{12} \text{ cm}^{-2}$ expected for the SiO₂/MoSe₂/hBN sample, and we observe an asymmetric exponential tail developing at high temperature. By contrast, in Fig. 3b, the doping density has been fixed to $0.7 \times 10^{12} \text{ cm}^{-2}$. This corresponds to the carrier density expected in the GaInP/MoSe₂/hBN sample and has been estimated by comparing the temperature dependence of the repulsive and attractive polaron energy splitting (see Supplementary information Fig. S2). Here, we observe that, over the entire temperature range considered, the emission PL profile of the attractive Fermi polaron resonance remains symmetric and can be well fitted with Gaussians (dashed lines), indicating that the attractive polaron persists as a well-defined quasiparticle. We also calculated the reliance of PL lineshape on the doping density at 50 K, and find the suppression of recoil effect with doping (Fig. S3).

Temperature dependent PL spectra assigned to trion emission in the SiO₂/MoSe₂/hBN sample are shown in Fig. 3c. All spectra are normalized with respect to their maximum intensity. As we ramp the temperature from 4 K to 50 K, a distinct low-energy tail becomes visible at the emission peaks for the case of trion photoluminescence. The strong deviation from a Gaussian fit (dashed line) is evident at 50 K. In striking contrast, the AP PL from the GaInP/MoSe₂/hBN sample as exhibited in Fig. 3d, only shows a slight spectral broadening, without any signs of asymmetry as temperature increases. This is evidenced by the excellent match to a Gaussian fit at 50 K, implying the disappearance of the recoil effect. Thus, besides the absorption characteristics (see also Fig. S2), the temperature-dependent PL provides another clear distinction between trions and AP.

Conclusions

Our study reveals the formation of attractive Fermi polarons at the GaInP/MoSe₂ hybrid interface, which emerges as the dominant feature in photoluminescence, with a characteristic dependence on temperature. Due to the integration of TMDC monolayers with epitaxially grown surfaces, we observe a strong reduction of dielectric disorder, giving rise to enhanced optical properties, such as luminescence with strongly suppressed disorder-related broadening. We demonstrate a considerable charge-doping mechanism at the GaInP/MoSe₂ interface, which results in a significant transfer of optical oscillator strength to the attractive Fermi polaron resonance. We show that, in contrast to the low-doping regime, the low-energy carrier-recoil exponential tail is suppressed in temperature-dependent photoluminescence, consistent with the attractive polaron

remaining a well-defined quasiparticle at temperatures below the Fermi energy. Furthermore, the presence of both repulsive and attractive polarons in reflectance, along with the temperature dependence of their energy splitting, matches the predicted behavior of polaron quasiparticles. Our findings are important for engineering mixtures of excitons and charge carriers in hybrid structures, e.g., in combined optics-transport experiments.

Methods

Sample and experimental setup

The MoSe₂ monolayers were exfoliated from crystals grown by chemical vapor deposition, and deposited on the substrates via a standard dry viscoelastic transfer method⁴⁸. The SiO₂ substrates used in this study consist of a 90 nm-thick SiO₂ layer on top of a silicon wafer. The GaInP substrates were made of a 10 nm-thick lattice-matched Ga_{0.51}In_{0.49}P layer grown on an AlAs/AlGaAs distributed Bragg reflector (DBR) via molecular beam epitaxy (Fig. 1a). The DBR not only enhances the light output, but also allows for straightforward absorption measurements in the back-reflection geometry. Substrates used for tunneling spectroscopy were grown via the same method, but lack the DBR to enhance their electric conductivity. Additionally, we produced a sample where the MoSe₂ flake was covered with a thin layer (~10 nm) of hBN and subsequently annealed at 400 °C in an Ar:H₂ atmosphere (95:5 ratio) for 2 hours. The STM experiments were performed in an ultrahigh vacuum chamber at 100 K, using chemically etched Au tips. Differential conductance spectroscopy was performed with a lock-in amplifier at 1356 Hz and 14 mV modulation frequency. The samples were degassed at 500 K for 1h prior to measurements.

Computational Details

To compare with and interpret the experimental PL profiles shown in Fig. 3, we employ a finite-temperature Fermi polaron theory^{46, 47} that goes beyond trion-based theories⁴¹⁻⁴³. Our theory assumes uncorrelated thermalized excitons and a thermal distribution of charge carriers. Within these approximations, the photoluminescence, $PL(\omega)$, at frequency ω (measured from the exciton) is proportional to the exciton spectral function via the Kennard-Stepanov relation⁴⁹⁻⁵¹, $PL(\omega) = e^{-\beta\omega} A(\omega)$. Here, the exciton spectral function $A(\omega) = -(1/\pi)Im G(\omega + i0^+)$ depends on the exciton Green's function $G(\omega) = [\omega - \Sigma(\omega)]^{-1}$ (we work in units where the reduced Planck constant is 1). The details of the many-body dressing of excitons by the charge carriers are contained within the self energy $\Sigma(\omega)$, and, for PL close to the exciton and trion, this is in turn dominated by processes involving at most a single carrier together with the exciton. Within this approximation we have $\Sigma(\omega) = \sum_{\mathbf{k}} f_{\mathbf{k}} T(k, \omega + \epsilon_{\mathbf{k}})$, with k the carrier momentum, $\epsilon_{\mathbf{k}} = k^2/(2m)$ its dispersion, $\epsilon_k^X = k^2/(2m_X)$ the exciton dispersion, and $f_{\mathbf{k}}$ the Fermi-Dirac distribution of charges at the given temperature. Importantly, the distribution function in the self energy is responsible for the characteristic recoil effect that occurs at either low doping or high temperature, in agreement with trion-based theory⁴¹⁻⁴³. The low-energy scattering T matrix of excitons and electrons close to the trion resonance is given by $T^{-1}(\mathbf{q}, \omega) = -\sum_{\mathbf{k}} \frac{1}{\epsilon_T + \epsilon_{\mathbf{k}} + \epsilon_k^X} - \sum_{\mathbf{k}} \frac{1-f_{\mathbf{k}}}{\omega - \epsilon_{\mathbf{k}} - \epsilon_{\mathbf{k}-\mathbf{q}}^X + i0^+}$ ⁴⁶,

⁴⁷. The theoretical PL spectra are convolved with a Lorentzian of FWHM linewidth of 8 meV, using $\epsilon_T = 22.5$ meV, and the MoSe₂ values of the exciton and carrier (hole) effective masses: $m_X = 1.15m_0$ and $m = 0.59m_0$ with m_0 the free electron mass. The exciton energy at zero temperature and vanishing doping is treated as a fitting parameter.

Acknowledgement

The authors gratefully acknowledge funding by Ministry of Research and Culture of Lower Saxony (MWK) within the project DyNano and the Wissenschaftsraum ELiKo. Support by the German Research Foundation (DFG) within the program INST 184/234-1 FUGG is acknowledged. C.C. and A.M.V. acknowledge additional support from MWK (Professorinnenprogramm für Niedersachsen) as well as from the German Ministry of Education and Research (Professorinnenprogramm III). The computational resources were provided by the computing cluster ROSA at the Carl von Ossietzky University of Oldenburg financed by MWK and by DFG (INST 184/225-1 FUGG). S.H. is grateful for financial support by the DFG (HO 5194/16-1). S.T acknowledges support from Applied Materials Inc. (materials synthesis), NSF CBET 2330110 (materials environmental testing), DOE-SC0020653 (TMDCs excitonic testing studies), and Lawrence Semiconductors (precursor purification). K.W. and T.T. acknowledge support from the JSPS KAKENHI (Grant Numbers 21H05233 and 23H02052) and World Premier International Research Center Initiative (WPI), MEXT, Japan. BCM, JL and MMP acknowledge support from the Australian Research Council through Discovery Projects DP240100569 (JL) and 250103746 (BCM, JL, MMP), and Future Fellowship FT200100619 (MMP). FMM acknowledges financial support from the Spanish Ministry of Science, Innovation and Universities through the “Maria de Maeztu” Programme for Units of Excellence in R&D (CEX2023-001316-M) and from the Ministry of Science, Innovation and Universities MCIN/AEI/10.13039/501100011033, FEDER UE, project No. PID2023-150420NB-C31 (Q).

References

1. Wang, G., et al. Colloquium: Excitons in atomically thin transition metal dichalcogenides. *Rev. Mod. Phys.* **90**, 021001 (2018).
2. Nuckolls, K. P., Yazdani, A. A microscopic perspective on moiré materials. *Nat. Rev. Mater.* **9**, 460-480 (2024).
3. Mak, K. F., Shan, J. Semiconductor moiré materials. *Nat. Nanotechnol.* **17**, 686-695 (2022).
4. Mak, K. F., Shan, J. Photonics and optoelectronics of 2D semiconductor transition metal dichalcogenides. *Nat. Photon.* **10**, 216-226 (2016).
5. Xia, F., Wang, H., Xiao, D., Dubey, M., Ramasubramaniam, A. Two-dimensional material nanophotonics. *Nat. Photon.* **8**, 899-907 (2014).
6. Drüppel, M., Deilmann, T., Krüger, P., Rohlfing, M. Diversity of trion states and substrate effects in the optical properties of an MoS₂ monolayer. *Nat. Commun.* **8**, 2117 (2017).
7. Raja, A., et al. Dielectric disorder in two-dimensional materials. *Nat. Nanotechnol.* **14**, 832-837 (2019).
8. Klein, J., et al. Impact of substrate induced band tail states on the electronic and optical properties of MoS₂. *Appl. Phys. Lett.* **115**, 261603 (2019).
9. Kutrowska-Girzycka, J., et al. Exploring the effect of dielectric screening on neutral and charged-exciton properties in monolayer and bilayer MoTe₂. *Appl. Phys. Rev.* **9**, 041410 (2022).
10. Shao, F., et al. Substrate influence on transition metal dichalcogenide monolayer exciton absorption linewidth broadening. *Phys. Rev. Mater.* **6**, 074005 (2022).
11. Waldherr, M., et al. Observation of bosonic condensation in a hybrid monolayer MoSe₂-GaAs microcavity. *Nat. Commun.* **9**, 3286 (2018).

12. Sortino, L., *et al.* Bright single photon emitters with enhanced quantum efficiency in a two-dimensional semiconductor coupled with dielectric nano-antennas. *Nat. Commun.* **12**, 6063 (2021).
13. Mak, K. F., *et al.* Tightly bound trions in monolayer MoS₂. *Nat. Mater.* **12**, 207-211 (2013).
14. Ross, J. S., *et al.* Electrical control of neutral and charged excitons in a monolayer semiconductor. *Nat. Commun.* **4**, 1474 (2013).
15. Iff, O., *et al.* Substrate engineering for high-quality emission of free and localized excitons from atomic monolayers in hybrid architectures. *Optica* **4**, 669-673 (2017).
16. Lyons, T. P., *et al.* Giant effective Zeeman splitting in a monolayer semiconductor realized by spin-selective strong light–matter coupling. *Nat. Photon.* **16**, 632-636 (2022).
17. Venanzi, T., *et al.* Ultrafast switching of trions in 2D materials by terahertz photons. *Nat. Photon.* **18**, 1344-1349 (2024).
18. Massignan, P., Zaccanti, M., Bruun, G. M. Polarons, dressed molecules and itinerant ferromagnetism in ultracold Fermi gases. *Rep. Prog. Phys.* **77**, 034401 (2014).
19. Efimkin, D. K., MacDonald, A. H. Many-body theory of trion absorption features in two-dimensional semiconductors. *Phys. Rev. B* **95**, 035417 (2017).
20. Smoleński, T., *et al.* Interaction-Induced Shubnikov-de Haas Oscillations in Optical Conductivity of Monolayer MoSe₂. *Phys. Rev. Lett.* **123**, 097403 (2019).
21. Sidler, M., *et al.* Fermi polaron-polaritons in charge-tunable atomically thin semiconductors. *Nat. Phys.* **13**, 255-261 (2017).
22. Back, P., *et al.* Giant Paramagnetism-Induced Valley Polarization of Electrons in Charge-Tunable Monolayer MoSe₂. *Phys. Rev. Lett.* **118**, 237404 (2017).
23. Scazza, F., Zaccanti, M., Massignan, P., Parish, M. M., Levinsen, J. Repulsive Fermi and Bose Polarons in Quantum Gases. *Atoms* **10**, 55 (2022).
24. Alexandrov, A. S., Devreese, J. T. *Advances in Polaron Physics*. Springer Berlin, Heidelberg (2010).
25. Tan, L. B., *et al.* Interacting Polaron-Polaritons. *Phys. Rev. X* **10**, 021011 (2020).
26. Cotlet, O., Pientka, F., Schmidt, R., Zarand, G., Demler, E., Imamoglu, A. Transport of Neutral Optical Excitations Using Electric Fields. *Phys. Rev. X* **9**, 041019 (2019).
27. Chervy, T., *et al.* Accelerating Polaritons with External Electric and Magnetic Fields. *Phys. Rev. X* **10**, 011040 (2020).
28. Smoleński, T., *et al.* Signatures of Wigner crystal of electrons in a monolayer semiconductor. *Nature* **595**, 53-57 (2021).
29. Shimazaki, Y., *et al.* Optical Signatures of Periodic Charge Distribution in a Mott-like Correlated Insulator State. *Phys. Rev. X* **11**, 021027 (2021).
30. Zhang, L., *et al.* Wigner polarons reveal Wigner crystal dynamics in a monolayer semiconductor. arXiv:2512.16631 (2025).
31. Schwartz, I., *et al.* Electrically tunable Feshbach resonances in twisted bilayer semiconductors. *Science* **374**, 336-340 (2021).
32. Huber, O., *et al.* Optical control over topological Chern number in moiré materials. arXiv:2508.19063 (2025).
33. Klitzke, M., Schygulla, P., Klein, C., Kleinschmidt, P., Hannappel, T., Lackner, D. Optimization of GaInP absorber design for indoor photovoltaic conversion efficiency above 40%. *Appl. Phys. Lett.* **127**, 023301 (2025).
34. Wierzbowski, J., *et al.* Direct exciton emission from atomically thin transition metal dichalcogenide heterostructures near the lifetime limit. *Sci. Rep.* **7**, 12383 (2017).
35. Cadiz, F., *et al.* Excitonic Linewidth Approaching the Homogeneous Limit in MoS₂-Based van der Waals Heterostructures. *Phys. Rev. X* **7**, 021026 (2017).
36. Lübken, B., Nilius, N. Laser stimulation of MoSe₂/Au(111) in an STM junction: Photoinduced versus thermally induced current response. *Phys. Rev. B* **103**, 245420 (2021).

37. Zare Pour, M. A., *et al.* Band energy diagrams of n-GaInP/n-AlInP(100) surfaces and heterointerfaces studied by X-ray photoelectron spectroscopy. *Surfaces and Interfaces* **34**, 102384 (2022).

38. Dong, Y., Feenstra, R. M., Semtsiv, M. P., Masselink, W. T. Band offsets of InGaP / GaAs heterojunctions by scanning tunneling spectroscopy. *J. Appl. Phys.* **103**, 073704 (2008).

39. Yamusa, S. A., *et al.* Quasi-particle band structure and optical absorption in MoS₂: Impact of spin-orbit coupling and vdW corrections for photodetection application. *Phys. B Condens. Matter* **706**, 417074 (2025).

40. Yamusa, S. A., *et al.* Enhanced DFT predictions of the structural and optoelectronic properties of MoTe₂ for high performance photodetection: Application to GW-based functionals and Hubbard U and V corrections. *Chem. Phys.* **573**, 112018 (2023).

41. Zipfel, J., *et al.* Electron recoil effect in electrically tunable MoSe₂ monolayers. *Phys. Rev. B* **105**, 075311 (2022).

42. Esser, A., Runge, E., Zimmermann, R., Langbein, W. Photoluminescence and radiative lifetime of trions in GaAs quantum wells. *Phys. Rev. B* **62**, 8232-8239 (2000).

43. Esser, A., Zimmermann, R., Runge, E. Theory of Trion Spectra in Semiconductor Nanostructures. *Phys. Status Solidi B* **227**, 317-330 (2001).

44. Ajayi, O. A., *et al.* Approaching the intrinsic photoluminescence linewidth in transition metal dichalcogenide monolayers. *2D Mater.* **4**, 031011 (2017).

45. Martin, E. W., *et al.* Encapsulation Narrows and Preserves the Excitonic Homogeneous Linewidth of Exfoliated Monolayer MoSe₂. *Phys. Rev. Appl.* **14**, 021002 (2020).

46. Mulkerin, B. C., Tiene, A., Marchetti, F. M., Parish, M. M., Levinsen, J. Exact Quantum Virial Expansion for the Optical Response of Doped Two-Dimensional Semiconductors. *Phys. Rev. Lett.* **131**, 106901 (2023).

47. Tiene, A., Mulkerin, B. C., Levinsen, J., Parish, M. M., Marchetti, F. M. Crossover from exciton polarons to trions in doped two-dimensional semiconductors at finite temperature. *Phys. Rev. B* **108**, 125406 (2023).

48. Andres, C.-G., *et al.* Deterministic transfer of two-dimensional materials by all-dry viscoelastic stamping. *2D Mater.* **1**, 011002 (2014).

49. Kennard, E. H. On The Thermodynamics of Fluorescence. *Phys. Rev.* **11**, 29-38 (1918).

50. Stepanov, B. I. A Universal Relation Between the Absorption and Luminescence Spectra of Complex Molecules. *Sov. Phys. Dokl.* **2**, 81 (1957).

51. McCumber, D. E. Einstein Relations Connecting Broadband Emission and Absorption Spectra. *Phys. Rev.* **136**, A954-A957 (1964).